2020 IEEE International Conference on Systems, Man, and Cybernetics (SMC)
October 11-14, 2020. Toronto, Canada

Electrical Impedance Tomography using Differential Evolution integrated with a Modified Newton Raphson Algorithm

Rick Hao Tan, and Carlos Rossa
Faculty of Engineering and Applied Science
Ontario Tech University, Oshawa, ON, Canada
hao.tan1@ontariotechu.net; carlos.rossa@ontariotechu.ca

***Abstract*—Electrical impedance tomography (EIT) is a non-invasive medical imaging procedure. Image reconstruction in EIT is difficult because it involves solving a non-linear and ill-posed mathematical problem. One of the most commonly implemented inverse approaches is usually a variation of the Newton Raphson algorithm. However, this approach is not guaranteed to reach a global optimum or a local optimum and as such, it requires an accurate initial estimation of the resistance distribution, which is not always available in practice.**

In this paper, a new method is proposed to solve for the inverse problem in EIT while avoiding dependencies on the initial estimation of the resistance distribution. The proposed approach uses a differential evolution (DE) optimizer integrated with the Newton Raphson algorithm. The stochastic nature of DE allows the problem to be solved without having an accurate initial estimation and allows for solutions that will not be trapped in local minimal values. Simulation results indicate that the proposed approach outperforms the traditional differential evolution algorithm, and performs similarly to the traditional Modified Newton Raphson algorithm with accurate initial estimation. The proposed method does, however, have an advantage over the Modified Newton Raphson algorithm as it does not require an estimate of the initial resistance distribution.

***Index Terms*—Electrical impedance tomography; differential evolution; Modified Newton Raphson.**

I. Introduction

Electrical impedance tomography (EIT) is an inexpensive and non-invasive way of conducting medical imaging when compared to traditional methods like X-Ray and Magnetic Resonance Imaging (MRI) [1], [2]. EIT is able to provide an image of the conductivity distribution of the tissue being examined. The produced image can assist health officials in in a variety of applications such as cranial imaging of newborns, lung imaging, hyperthermia treatment, breast imaging, amongst many others [3]–[6]. Although the resolution of EIT is not as advanced as X-Ray or MRI, it is more pleasant for the patient as it only involves placing electrodes on the periphery of the body [7].

EIT reconstructs the resistivity or conductivity distribution of the tissue under test by applying electric current through a given pair of electrodes and observing the induced voltage across the other ones. From the current-voltage data, an image is created based on the reconstructed resistivity distribution that satisfies the voltage-current relationship.

The conductivity distribution inside the body of interest can be termed as $\sigma(\vec{x})$, where $\vec{x}$ is the voxel position. Electrical current only flows inside the medium ζ and the voltage distribution inside ζ is $U(\vec{x})$. Solving the problem of EIT usually requires two approaches: the forward solution as well as the inverse solution [8]. The forward solution calculates the boundary voltages of ζ given an initial $\sigma(\vec{x})$, whereas the inverse problem is to calculate $\sigma(\vec{x})$ while knowing the boundary voltages.

In mathematical terms, the forward solution is defined as:

$$U_b(\vec{y}) = f(I(\vec{y}), \sigma(\vec{x})), \ \forall \vec{y} \in \partial\zeta \wedge \vec{x} \in \zeta. \tag{1}$$

In other words, if a current $I(\vec{y})$, is applied to ζ, find the induced voltages $U_b(\vec{y})$ given a known resistivity distribution $\sigma(\vec{x})$. The inverse solution is posed as:

$$\sigma(\vec{x}) = f^{-1}(I(\vec{y}), U_b(\vec{y})), \ \forall \vec{y} \in \partial\zeta \wedge \vec{x} \in \zeta. \tag{2}$$

More specifically, given the applied boundary current $I(\vec{y})$, find the conductivity $\sigma(\vec{x})$ that gives the measured boundary voltages $U_b(\vec{y})$.

Finding the solution to (2) is not always a trivial task [9]. The inverse solution is ill-posed if the amount of unknown parameters exceed the amount of unique voltage measurements [8]. Hence, there can exist multiple $\sigma(\vec{x})$ solutions for a given set of boundary voltage values and determining the true resistance distribution amongst all possible solutions is the challenge of EIT. Usually, the two approaches of (1) and (2) are implemented together in an iterative fashion to solve for the true resistance distribution.

A comprehensive review on different methods to solve the forward and inverse solution can be found in [10], [11]. Most of these methods can be broadly classified into

We acknowledge the support of the Natural Sciences and Engineering Research Council of Canada (NSERC), the Canadian Institutes of Health Research (CIHR), and the Social Sciences and Humanities Research Council of Canada (SSHRC), [funding reference number NFRFE-2018-01986].

Cette recherche a été financée par le Conseil de recherches en sciences naturelles et en génie du Canada (CRSNG), par les Instituts de recherche en santé du Canada (IRSC), et par le Conseil de recherches en sciences humaines du Canada (CRSH), [numéro de référence NFRFE-2018-01986].

deterministic and stochastic approaches. Methods to solve for the forward solution typically fall in the first category and include Kirchoff's current law, finite element modelling, boundary element methods, and linear box-approaches [12]–[15]. For the inverse solution, deterministic methods such as the Modified Newton Raphson (MNR), perturbation method, sensitivity theorem, and block approach have been proposed [16]–[21]. Evolutionary methods such as differential evolution (DE) and particle swarm optimization are examples of stochastic approaches used to set up the inverse formulation of ill-posed problems [22]–[24]. More recent advances in computational resources has given rise to intelligent machine learning algorithms. The problem of electrical impedance tomography has also been reconstructed by using methods like Convolutional Neural networks [14], [25]–[27] and Bayesian Learning [28]. However, these algorithms require a complex network as well as an extensive training period and testing data.

Deterministic methods generally achieve a solution in a faster time frame than computationally heavy stochastic and intelligent algorithms such as differential evolution [29]. However, deterministic methods require an accurate initial estimation of the resistivity distribution $\sigma(\vec{x})$ in order to converge to a global optimum. It has been reported that the initial guess for the well-known MNR algorithm for example must be within a range of 0.1 to 10 times the average magnitude of the true resistivity [16]. This may not always be feasible as information required to make the initial estimation may not be available. A popular alternative to MNR are the so-called perturbation methods, which make use of an approximation of a Jacobian matrix that is known to not always lead to convergence when compared to MNR [17], [18]. On the other hand, stochastic methods are more effective in the sense that they generate random solutions to avoid convergence in local minima [30]. However, convergence takes an excessively long time to obtain feasible results, particularly when trying to identify an area of focus within an unknown medium. Thus, a hybrid solution combining MNR and a stochastic method is suitable.

In this paper, a novel algorithm that integrates differential evolution with the Modified Newton Raphson algorithm is presented. It is a hybrid approach. The proposed method uses MNR to optimize the candidate solutions obtained from DE before they are considered for further iterations. The hybrid algorithm does not require an accurate initial estimation $\sigma(\vec{x})$ to converge to a potential solution. It is also able to generate successful results in a shorter time frame than DE. The contributions of this paper is an optimization algorithm that: (1) implements the Modified Newton Raphson algorithm to optimize the mutated solutions of the differential evolution algorithm and (2) also dictates the crossover factor of the algorithm depending on the fitness of the optimized mutated solution. Hybrid methods combining stochastic and deterministic methods have been proposed before. A paper implementing both DE and the MNR algorithm to solve the problem of EIT was published by Li et al [29]. In their approach, the DE algorithm executes once to find a suitable initial resistance estimation to the EIT problem. Immediately following, they implemented the MNR algorithm with the found initial resistance estimation to solve for a final converged solution. Their approach only executes DE and MNR once, in a successive fashion. The output of the DE is the input for the MNR algorithm. The final solution then heavily relies on the output of the DE algorithm to generate a suitable initial resistance distribution. The DE algorithm may not always generate a suitable initial resistance distribution. This paper's approach has the ability to optimize every individual within the DE algorithm's population using MNR. Therefore, there is a higher chance of a successfully converged final solution because the individuals in the population will have been optimized by the MNR algorithm.

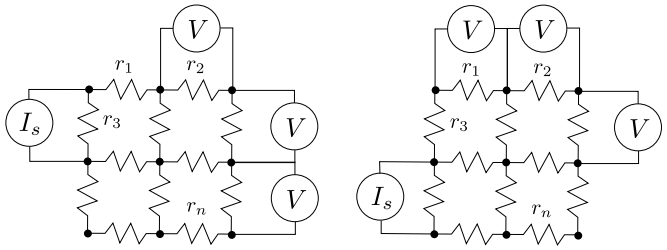

Fig. 1: Simplified electrical resistor grids with different injected current I_s and voltage measurement patterns at the grid boundary.

This paper is structured as follows: Section II outlines the mathematical foundation of the Modified Newton Raphson algorithm. It is then followed by the background of the differential evolution algorithm in Section III. The integrated hybrid approach is presented in Section IV, which is then followed by simulation results and conclusions.

II. Modified Newton Raphson Algorithm

The conductivity distribution, $\sigma(\vec{x})$, can be discretized in a finite number of resistive elements and modelled as a square resistor grid with resistors arranged in horizontal and vertical fashion as shown in Fig. 1. Each resistor can be represented as having a resistance r and the size of the square resistor grid is $s \times s$, where s is the number of horizontal nodes in the resistor grid. The circuit is excited with an injected current of known magnitude through different pairs of boundary electrodes. The current flowing through a given pair of electrodes induces a voltage at the remaining electrodes. Boundary voltage measurements are then taken at different electrode pairs. The different injection current patterns and measurements patterns determine how many unique measurements there are for a given resistor grid.

Using Kirchhoff's current law, the sum of the currents at every node of the resistor grid can be used to establish a mathematical relationship between the voltages, resistance and injected current at every node. Once the equations are arranged in a matrix format, the forward solution (1) can be represented as:

$$\mathbf{U_b} = \mathbf{C}^{-1}\mathbf{I} \tag{3}$$

where $\mathbf{U_b} \in \mathbb{R}^{s^2 \times 1}$, is a column vector that holds all the boundary voltages. The matrix $\mathbf{C} \in \mathbb{R}^{s^2 \times s^2}$ is the conductivity matrix (the inverse of electrical resistivity) and $\mathbf{I} \in \mathbb{R}^{s^2 \times 1}$ is a vector that holds all the injected currents patterns in a given pair of nodes located in the boundary of the resistor grid [17].

The Modified Newton Raphson approach iteratively updates the initial conductivity distribution input until the calculated boundary voltages match the measured boundary voltage for a given current injection input. The update to the resistance distribution can be summarized as:

$$\mathbf{r}^{k+1} = \mathbf{r}^k + \Delta\mathbf{r}^k. \tag{4}$$

In (4), $\mathbf{r}^k \in \mathbb{R}^{1\times(2s^2-2s)}$ is the current resistance distribution at iteration k, $\Delta\mathbf{r}^k$ is the calculated change to be applied to the resistance distribution and $\mathbf{r}^{k+1}$ is the updated resistance distribution. The MNR iterative procedure stops when $\Delta\mathbf{r}^k$ is smaller than a predetermined tolerance value. Once the iterative procedure has stopped, it is assumed that the algorithm has converged to a final solution of $\mathbf{r}$, which is a possible solution that represents the true resistance distribution of the medium, provided that the problem is well posed and the initial guess $\mathbf{r}^0$ is accurate.

To start the MNR algorithm, an initial resistivity distribution $\mathbf{r}^0$ needs to be specified. The values of $\mathbf{r}^0$ are crucial as they determine whether the algorithm can successfully converge to a solution or not. If $\mathbf{r}^0$ is very different from the true resistance distribution $\mathbf{r_t}$, then the algorithm will not converge. It is found that if $|\mathbf{r}^0 - \mathbf{r_t}| < 10$, then the converged solution is generally acceptable [16]. Therefore, it is crucial to have a good starting $\mathbf{r}^0$ to initialize the MNR algorithm. This is the main limitation of implementing the MNR algorithm.

To calculate the resistance updates, $\Delta\mathbf{r}^k$, an error term is required. The error is defined as the least mean square error between the calculated and observed boundary voltages given at every iteration as:

$$\theta(\mathbf{r}^k) = \frac{1}{2}\left[\mathbf{V}(\mathbf{r}^k) - \mathbf{V}_0(\zeta)\right]^T\left[\mathbf{V}(\mathbf{r}^k) - \mathbf{V}_0(\zeta)\right] \tag{5}$$

where $\mathbf{V} \in \mathbb{R}^{n\times p}$ is a matrix that holds all the calculated boundary voltages given $\mathbf{r}^k$ for all the different injection current patterns [17]. The variable n represents the amount of boundary electrodes and p represents the amount of current injection patterns. Likewise, $\mathbf{V}_0 \in \mathbb{R}^{n\times p}$ are the respective measured boundary voltages.

In order to find a solution $\mathbf{r}_k$ that minimizes the error between $\mathbf{V}$ and $\mathbf{V_0}$, (5) is differentiated with respect to $\mathbf{r}^k$ and set equal to 0 [17]:

$$\frac{\partial\theta}{\partial\mathbf{r}^k} = \frac{\partial\mathbf{V}}{\partial\mathbf{r}^k}^T[\mathbf{V} - \mathbf{V}_0] = 0, \text{ or} \tag{6}$$

$$\theta' = [\mathbf{V}']^T[\mathbf{V} - \mathbf{V}_0] = 0. \tag{7}$$

In (7), the term $\mathbf{V}' = \partial\mathbf{V}/\partial\mathbf{r}^k \in \mathbb{R}^{2s^2-2s\times n}$ is the Jacobian matrix representing the rate of the change of the calculated boundary voltages with respect to each of the resistors in $\mathbf{r}^k$.

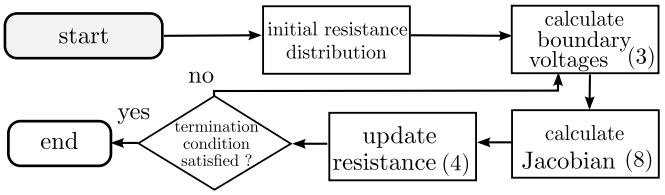

Fig. 2: The MNR algorithm starts with an initial resistance distribution $\mathbf{r}^0$ and calculates the required resistance updates $\Delta\mathbf{r}^k$ to apply upon itself. After running through the algorithm for a prescribed amount of iterations, the algorithm may converge to a global solution if the initial resistance estimation $\mathbf{r}^0$ is close to the true resistance distribution $\mathbf{r_t}$.

The general form of the Jacobian matrix can be seen as:

$$[\mathbf{V}'] = \begin{bmatrix} \frac{\partial V_1}{\partial r_1} & \frac{\partial V_2}{\partial r_1} & \cdots & \frac{\partial V_n}{\partial r_1} \\ \frac{\partial V_1}{\partial r_2} & \frac{\partial V_2}{\partial r_2} & \cdots & \frac{\partial V_n}{\partial r_2} \\ \vdots & \vdots & \ddots & \vdots \\ \frac{\partial V_1}{\partial r_{2s^2-2s}} & \cdots & \cdots & \frac{\partial V_n}{\partial r_{2s^2-2s}} \end{bmatrix}. \tag{8}$$

Since (7) is a nonlinear function of $\mathbf{r}$, a Taylor series expansion is taken on (7) about an arbitrary point $\mathbf{r} = \mathbf{r}^k$. Thus (7) can be approximated as:

$$\theta' \approx \theta'(\mathbf{r}^k) + \theta''(\mathbf{r}^k)\Delta\mathbf{r}^k. \tag{9}$$

The term $\theta'' = \partial^2\mathbf{V}/\partial\mathbf{r}^2$ is the Hessian matrix given by [17]:

$$\theta'' \approx [\mathbf{V}']^T[\mathbf{V}']. \tag{10}$$

To isolate for $\Delta\mathbf{r}^k$, (7) and (10) are substituted into (9) to yield:

$$\Delta\mathbf{r}^k = \left\{[\mathbf{V}'(\mathbf{r}^k)]^\mathbf{T}\mathbf{V}'(\mathbf{r}^k) + \lambda\mathbf{W}\right\}^{-1}[\mathbf{V}'(\mathbf{r}^k)][\mathbf{V}(\mathbf{r}^k) - \mathbf{V}_0].$$

In the above, $\mathbf{W}$ is an identity matrix and $\lambda \in \mathbb{R}^+ \to 0$ is a scalar. Together, $\mathbf{W}$ and λ are added to the original formulation to mitigate the ill-conditioning of the problem and prevent the system from reaching singularity when performing the inverse [17], [31]. The resistance update term $\Delta\mathbf{r}^k$ is then used in (4) to calculate the updated resistance distributions. The flowchart in Fig. 2 illustrates the workflow of the Modified Newton Raphson algorithm.

III. Differential Evolution Algorithm

Differential evolution is a population based stochastic optimization algorithm that aims to find the global optimum solution of a given objective function [32]. The algorithm starts with a randomly initialized population of candidate solutions (individuals). Through various generations, the population is evolved via repeated evaluations of the objective function. The individual in the final population with the lowest objective function (fitness value) is often deemed as the solution. The random nature of the algorithm avoids local minima convergence. The single objective minimization problem may be stated as follows:

$$q(\mathbf{r_t}) = \min\theta(\mathbf{r}_i), \mathbf{r}_i \in \mathbf{P} \mid \mathbf{P}(i,j) = [L_j, D_j] \tag{11}$$

where q is the final fitness value, $\theta(\mathbf{r}_i)$ is the objective function as in (5) and $\mathbf{r}_i$ is a vector that represents individual i in the population [32]. Similar to MNR, each i^{th} individual is a vector string $\mathbf{r}_i \in \mathbb{R}^{1\times(2s^2-2s)}$ that holds all the resistor values in the resistor mesh. All the individuals are stored in a 2-dimensional matrix, $\mathbf{P} \in \mathbb{R}^{\pi\times(2s^2-2s)}$, where π is the number of individuals in the population. Thus, row i of $\mathbf{P}$ contains the i^{th} individual in the population while each column j of $\mathbf{P}$ contains all resistors j for all individuals. The global optimum solution is $\mathbf{r_t}$, while L and D are the lower and upper bounds of each resistor in $\mathbf{r}$. Differential evolution algorithms have 5 distinct steps [32]:

Population and parameter initialization: The initial parameters of the algorithm are set. This includes: number of individuals in the population π, number of generations γ, number of runs ρ, mutation factor ψ, and crossover factor ϵ. Both the mutation factor (ψ) and crossover factor (ϵ) are numbers that range from [0 1]. Random initial individuals $\mathbf{r}_i$ are generated within a given range [L D] to form the initial population of $\mathbf{P}_0$.

Mutation: Mutation takes place after the initial population is established. It is a crucial step to evolution as it introduces further randomness to the initial population so local minima are avoided. Mutation helps generate new mutated individuals that were not originally created during the initialization step. For each individual in the population, a mutant vector is generated. There are different formats of mutant vectors. In this study, the "DE/rand/1" format is selected [32]:

$$\mathbf{h} = \mathbf{r}_a + \psi(\mathbf{r}_b - \mathbf{r}_c) \tag{12}$$

In (12), $\mathbf{h}$ is the mutant vector, ψ is the mutation factor defined in Step 1, and $\mathbf{r}_a$, $\mathbf{r}_b$ and $\mathbf{r}_c$ are randomly selected individuals from $\mathbf{P}$. If ψ is large, the mutation is said to be large and the mutated vector $\mathbf{h}$ will be significantly different from any of the individuals in $\mathbf{P}$.

Crossover: The crossover follows the form of Binomial Crossover [33]. The crossover vector $\mathbf{z}$ is generated based on a random number c $\in$ [0 1]. The act of the crossover itself depends on the crossover factor ϵ set during Step 1. This process limits how much of the mutation vector $\mathbf{h}$ will be moved forward to evaluation in the next step. The larger ϵ the more likely $\mathbf{z}$ will resemble $\mathbf{h}$. On the contrary, the smaller ϵ is, the less likely $\mathbf{z}$ will resemble $\mathbf{h}$. The variable ι is a random number $\iota \in [1\ 2s^2 - 2s]$. Its purpose is to guarantee that at least one crossover is executed. The crossover is

$$\mathbf{z}_{i,j} = \begin{cases} \mathbf{h}_{i,j} & \text{if c} \leq \epsilon \text{ or j = } \iota \\ \mathbf{r}_{i,j} & \text{otherwise} \end{cases}. \tag{13}$$

For every j^{th} resistor in $\mathbf{r}_i$, a new c is generated.

Selection: The crossover vector $\mathbf{z}$ is compared against the target vector $\mathbf{r}_\gamma$ in the current generation to determine which is more fit to be survived into the next generation ($\gamma+1$). The process can be demonstrated by (14).

$$\mathbf{r}^{\gamma+1} = \begin{cases} \mathbf{z} & \text{if } f(z) < f(r^\gamma) \\ \mathbf{r}^\gamma & \text{otherwise} \end{cases}. \tag{14}$$

Repeat: The algorithm repeats the mutation, crossover, and selection stages until the maximum amount of iteration (generations) is reached. The most fit individual in the population of the last generation is the found optimum solution given the initialized parameters.

IV. Differential Evolution Integrated with Newton Raphson Algorithm

Although the Modified Newton Raphson and differential evolution algorithms both serve as potential solvers for the problem of EIT, they each have their own drawbacks. The MNR algorithm requires an accurate initial estimation to ensure convergence of the final solution. This is not always feasible as the medium being imaged is often unknown and an accurate initial estimation is not easily obtained. The DE algorithm does not require an accurate initial resistance estimation, however, it has difficulty identifying areas of higher resistance within the medium, in a short time frame.

In the proposed approach, the MNR algorithm is embedded into the DE algorithm. The objective function of the proposed algorithm is similar to (5) where the output is the difference between the calculated boundary voltages and the measured boundary voltages. In this hybrid approach, there are two significant differences than traditional DE. First, the hybrid approach optimizes the solutions of regular DE using MNR. Second, the crossover process is dynamic and depends on the fitness of the individual being evaluated.

The MNR algorithm is integrated into the mutation step of differential evolution. Instead of (12) as the mutant vector, the output of (12) is entered into (4) as the initial resistance distribution, $\mathbf{r}^0$. And after k iterations, the output is the new mutant vector, $\mathbf{h}_*$. The new mutant vector $\mathbf{h}_*$ in (15) is then used in the subsequent steps of DE in the Crossover and Selection stages.

$$\mathbf{h}_*^{k+1} = \mathbf{h}_*^k + \Delta\mathbf{h}_*^k \tag{15}$$
$$\text{Given: } \mathbf{h}_*^1 = \mathbf{r}_a + \psi(\mathbf{r}_b - \mathbf{r}_c)$$

Each individual in the population would have a evaluated fitness value associated with it. The fitness value of each individual is calculated using (5).

The crossover factor is also varied and not fixed in the proposed algorithm. In traditional DE, the crossover factor is a fixed value denoted by ϵ as shown in (13). However, in the proposed approach, the new crossover factor, β, switches between 0.1 and 0.9 depending on the fitness of the output of the Modified Newton Raphson algorithm, $\mathbf{h}_*^k$. As discussed in Section II, the MNR algorithm will not converge when the initial resistance distribution $\mathbf{r^0}$ is very different from $\mathbf{r_t}$. When MNR does not converge, the output is very unstable and can have chaotic values of 100 times that of $\mathbf{r_t}$. Thus, if $\mathbf{h}_*^1$ is

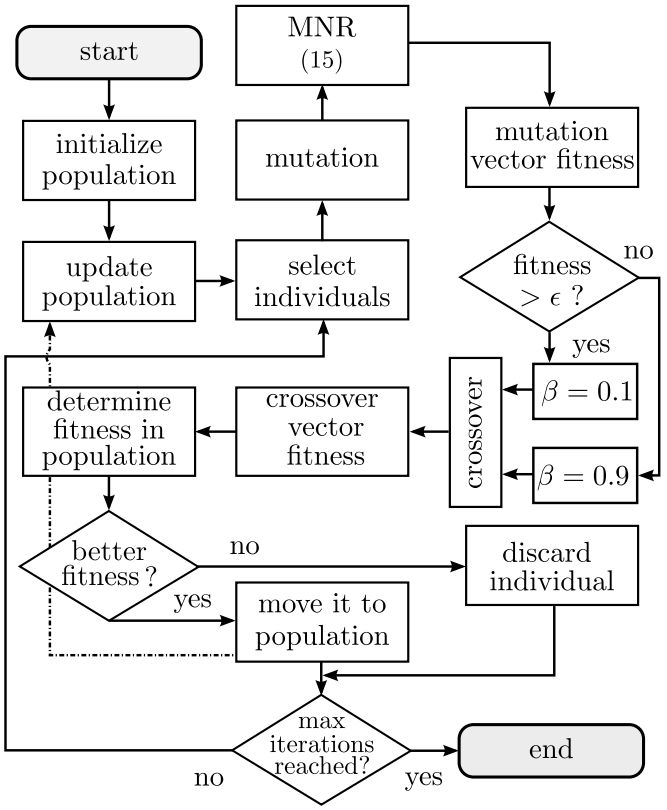

Fig. 3: The proposed system integrates the Modified Newton Raphson algorithm into a traditional differential evolution algorithm.

very different from $\mathbf{r_t}$, then $\mathbf{h}_*^k$ can be extremely inaccurate. In which case, the new crossover factor β is defined as 0.1, where minimal crossover occurs and most of the crossover vector $\mathbf{z}$ will be comprised of values from the values of the individual being analyzed in the population. The individuals in the population have been constrained to have values between $[L\ D]$ and so the instability is controlled. This ensures that chaotic solutions will not be stored throughout the generations. Vice versa, if the output of MNR is acceptable, β is changed to 0.9 where significant crossover occurs and the new crossover vector $\mathbf{z}$ will be made up of values from $\mathbf{h}_*^k$. The output of MNR is deemed acceptable or not by calling upon the fitness function of (5). If the fitness value is above 0.1, then the output is deemed unstable and $\beta = 0.1$ and if the fitness value is less than 0.1 then $\beta = 0.9$. The overall procedure of the proposed algorithm is summarized in a flowchart displayed in Fig. 3.

V. Simulation and Results

The forward problem is implemented in an electrical resistor mesh of size 50 nodes by 50 nodes and 16 boundary electrodes. A sequence of 16 distinct current patterns of 1 A are injected in a given pair neighbouring electrodes, one pair at a time, while the induced voltage at the remaining electrodes is measured. In addition, to represent physical experimentation, noise is introduced into the system. Each boundary voltage

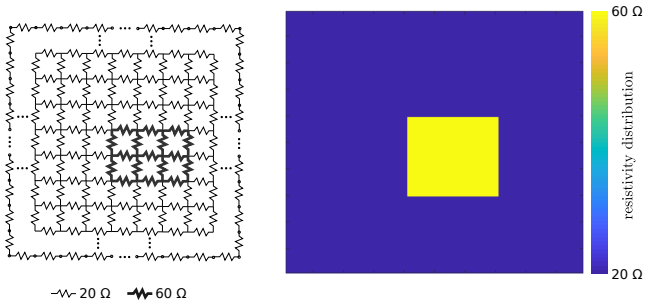

Fig. 4: The image output of the true resistance distribution is constructed from a 50 × 50 resistor grid and it shows a concentrated mesh of resistors with a higher resistance (60 Ω) than the rest of the resistors (20 Ω).

TABLE I: Simulations Parameters

Parameter	DE	Hybrid	MNR
Population (π)	50	50	N.A.
Generations (γ)	3600	36	N.A.
Mutation factor (ψ)	0.8	0.8	N.A.
Crossover factors (ϵ, β)	0.1	0.1/0.9	N.A.
Iterations of MNR	NA	7	7
Runs (ρ)	3	1	1

Note: N.A = Not Applicable

reading from the true distribution are injected with a randomized noise variation of 2%. The true distribution in the forward problem is represented by Fig. 4. The majority of the true distribution is constructed of 20 Ω resistors, where the middle of the mesh has a concentrated mesh of resistors at 60 Ω. The 60 Ω resistors in the middle of the mesh represent the anomaly within the medium that the EIT algorithms will attempt to identify and locate. For calculating the boundary voltage values of the true distribution, a custom script calculates the boundary voltages and the values are verified with LTSpice (electrical simulations software).

The inverse solution is modelled by an electrical grid of size 10 nodes by 10 nodes with 16 boundary electrodes. Current is injected through neighbouring paired electrodes in the resistor circuit, similar to Fig. 1 and voltage measurements are taken across the remaining electrode pairs.

The Modified Newton Raphson algorithm is executed with 3 different initial resistance distributions, i.e., 30 Ω (closest to true distribution), 70 Ω and 100 Ω. The results are then compared with the results of the differential evolution as well as the proposed algorithm, which do not rely on an accurate initial estimate of the resistivity distribution. The parameters for each of the simulations are listed in Table I and the obtained least square error between the induced boundary voltages in the measured and calculated models as defined in (5) are displayed in Table II.

Looking at the fitness values of Table II, it is apparent that the best solutions are generated by the hybrid method as well as the Modified Newton Raphson when a 30 Ω resistance

TABLE II: Simulated results. Fitness value defined in (5)

	MNR 30 Ω	MNR 70 Ω	MNR 100 Ω	DE	Hybrid
Fitness	0.167	60.72	386.8	82.9	0.199

distribution is used as the initial estimation. They yield the lowest fitness results of all the simulations, with MNR at 0.167 and hybrid at 0.199. A low fitness value means that the solved boundary voltage values of the 10 by 10 resistor grid closely resemble that of the true measured boundary voltage values of the 50 by 50 resistor grid. This is as expected since the MNR algorithm with the 30 Ω initial distribution places it very close to the true distribution. Therefore, a optimal solution is very likely to converge.

Meanwhile, the solution generated from the MNR with a 70 Ω initial start is much worse than the solutions generated from the 30 Ω initial distribution, with a fitness value of 60.72. The solution generated from the 100 Ω initial start yielded very inaccurate results, with a fitness of 386.8. This is also expected as a very inaccurate initial estimation will lead to inaccurate results or lack of convergence [16]. The traditional differential evolution algorithm yielded a fitness value of 82.9, much higher than the MNR at 30 Ω and 70 Ω and the hybrid algorithm. It can be observed that by incorporating MNR into the DE algorithm, the fitness value decreases significantly when compared to the traditional DE algorithm. Given the noise added to the voltage measurements, it can be concluded that there is significant performance difference between the MNR and the hybrid method. However, the MNR requires a precise estimation of the resistivity distribution as its initial guess, which is not always feasible in practice.

The final image output of the different simulations are displayed in Fig. 5. It should be noted that the actual solved resistance values are not exact values when compared to the true distribution. For the generated solutions, the resistors values are normalized by the maximum resistance value in each solution and presented on a colored scale of 0 to 1.

As confirmed by Table II, the MNR and hybrid approaches generated the best solutions. The two approaches are able to identify the resistors concentrated in the center that had higher resistance values. The 70 Ω estimation of MNR is able to identify the higher resistance values in the center as well, but with relatively higher background inconsistencies in resistance values. The 100 Ω estimation of MNR does not converge and thus is not able to find an overall distribution. The differential evolution also does not converge as it cannot identify the higher resistance values. The difference in values were sufficient enough to identify the higher resistance values in the middle of the mesh for the MNR and hybrid cases.

VI. Conclusion

Different inverse approaches for EIT are analyzed in this paper and a new hybrid method integrating MNR into the differential evolution method is proposed. The performance of the Modified Newton Raphson algorithm is compared to a differential evolution algorithm as well as a differential evolution algorithm integrated with Modified Newton Raphson. The results indicate that the hybrid algorithm outperforms the differential evolution algorithm and performs just as well as a Modified Newton Raphson algorithm when the initial resistance estimation was close to the true distribution. The hybrid method does, however, require a longer processing time when compared to the MNR algorithm.

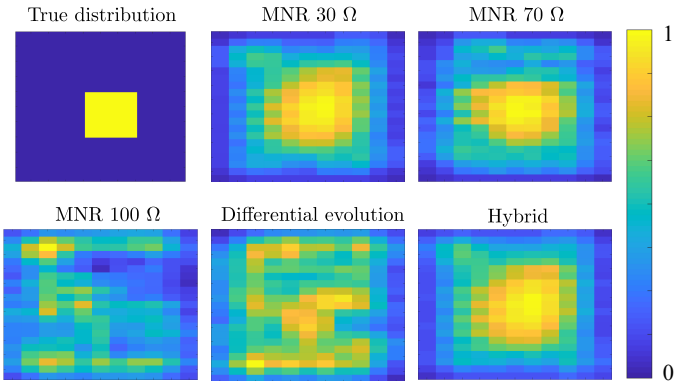

Fig. 5: The image output of each simulation is displayed, where the values are normalized between 0 and 1. The true distribution is constructed from a 50 × 50 resistor grid while the inverse solutions are constructed from a 10 × 10 resistor grid with 2% noise added to the boundary voltage readings.

The Modified Newton Raphson approach requires an accurate initial estimation to begin the algorithm and therefore, it is simulated with 30 Ω, 70 Ω and 100 Ω as the different initial resistance distributions. The true distribution is composed of mainly 20 Ω resistors, therefore, the initial estimation of 30 Ω for the Modified Newton Raphson algorithm produced optimal results. The other two estimations yielded subpar results.

The proposed hybrid algorithm is superior to the Modified Newton Raphson as it does not require a single well estimated guess to initialize the algorithm. The hybrid algorithm can produce the same results as the Modified Newton Raphson approach without any knowledge of the true distribution. Further simulations are to be conducted to explore the results of a more complex resistor grid. In addition, physical experiments will follow to confirm the results produced in this paper.

References

[1] T. A. Hughes, P. Liu, H. Griffiths, B. W. Lawrie, and C. M. Wiles, "An analysis of studies comparing electrical impedance tomography with x-ray videofluoroscopy in the assessment of swallowing." *Physiological measurement*, vol. 15 suppl 2a, pp. A199–A209, 1994. [Online]. Available: http://search.proquest.com/docview/76706803/

[2] J. L. Davidson, R. A. Little, P. Wright, J. Naish, R. Kikinis, G. J. M. Parker, and H. Mccann, "Fusion of images obtained from eit and mri," *Electronics Letters*, vol. 48, no. 11, pp. 1–2, 2012. [Online]. Available: http://search.proquest.com/docview/1616437493/

[3] J. Hough, A. Shearman, H. Liley, C. Grant, and A. Schibler, "Lung recruitment and endotracheal suction in ventilated preterm infants measured with electrical impedance tomography," *Journal of*

Paediatrics and Child Health, vol. 50, no. 11, pp. 884–889, 2014. [Online]. Available: http://search.proquest.com/docview/1635037861/

[4] P. Blankman, D. Hasan, M. Mourik, and D. Gommers, "Ventilation distribution measured with eit at varying levels of pressure support and neurally adjusted ventilatory assist in patients with ali," *Intensive Care Medicine*, vol. 39, no. 6, pp. 1057–1062, 2013.

[5] F. Ferraioli, A. Formisano, and R. Martone, "Effective exploitation of prior information in electrical impedance tomography for thermal monitoring of hyperthermia treatments," *IEEE Transactions on Magnetics*, vol. 45, no. 3, pp. 1554–1557, 2009.

[6] E. K. Murphy, A. Mahara, and R. J. Halter, "Absolute reconstructions using rotational electrical impedance tomography for breast cancer imaging," *IEEE Transactions on Medical Imaging*, vol. 36, no. 4, pp. 892–903, 2017.

[7] N. Hyvönen, H. Majander, and S. Staboulis, "Compensation for geometric modeling errors by positioning of electrodes in electrical impedance tomography," *Inverse Problems*, vol. 33, no. 3, p. 23, 2017.

[8] J. K. Seo, *Nonlinear inverse problems in imaging*. Chichester, West Sussex, U.K: John Wiley Sons Inc.

[9] D. Sbarbaro, M. Vauhkonen, and T. A. Johansen, "State estimation and inverse problems in electrical impedance tomography: observability, convergence and regularization," *Inverse Problems*, vol. 31, no. 4, p. 27, 2015.

[10] L. Borcea, "Electrical impedance tomography," *Inverse problems*, vol. 18, no. 6, p. R99, 2002.

[11] A. Adler and A. Boyle, "Electrical impedance tomography: Tissue properties to image measures," *IEEE Transactions on Biomedical Engineering*, vol. 64, no. 11, pp. 2494–2504, 2017.

[12] P. Zegarmistrz, S. A. Mitkowski, A. Porębska, and A. Dąbrowski, "Nodal analysis of finite square resistive grids and the teaching effectiveness of students ' projects," 2011.

[13] A. Gerami, "3d electrical resistivity forward modeling using the kirchhoff's method for solving an equivalent resistor network," *Journal of Applied Geophysics*, vol. 159, 08 2018.

[14] S. Ren, K. Sun, C. Tan, and F. Dong, "A two-stage deep learning method for robust shape reconstruction with electrical impedance tomography," *IEEE Transactions on Instrumentation and Measurement*, pp. 1–1, 2019.

[15] A. Abbasi and B. Vosoughi Vahdat, "Improving forward solution for 2d block electrical impedance tomography using modified equations," *Scientific Research and Essays*, vol. 5, pp. 1260–1263, 07 2010.

[16] T. Murai and Y. Kagawa, "Electrical impedance computed tomography based on a finite element model," *IEEE Transactions on Biomedical Engineering*, vol. BME-32, no. 3, pp. 177–184, March 1985.

[17] T. J. Yorkey, J. G. Webster, and W. J. Tompkins, "Comparing reconstruction algorithms for electrical impedance tomography," *IEEE Transactions on Biomedical Engineering*, vol. BME-34, no. 11, pp. 843–852, Nov 1987.

[26] S. J. Hamilton and A. Hauptmann, "Deep d-bar: Real-time electrical impedance tomography imaging with deep neural networks," *IEEE Transactions on Medical Imaging*, vol. 37, no. 10, pp. 2367–2377, 2018.

[18] Y. Kim, J. G. Webster, and W. J. Tompkins, "Electrical impedance imaging of the thorax," *J. Microwave Power*, vol. 18, pp. 245–257, 1983.

[19] D. B. Geselowitz, "An application of electrocardiographic lead theory to impedance plethysmography," *IEEE Transactions on Biomedical Engineering*, vol. BME-18, no. 1, pp. 38–41, 1971.

[20] J. Lehr, "A vector derivation useful in impedance plethysmographic field calculations," *IEEE Transactions on Biomedical Engineering*, vol. BME-19, no. 2, pp. 156–157, 1972.

[21] A. Abbasi and B. V. Vahdat, "A non-iterative linear inverse solution for the block approach in eit," *Journal of Computational Science*, vol. 1, no. 4, pp. 190–196, 2010.

[22] R. Ribeiro, A. Feitosa, R. Souza, and W. Dos Santos, "A modified differential evolution algorithm for the reconstruction of electrical impedance tomography images," 05 2014, pp. 1–6.

[23] W. Dos Santos, V. Barbosa, R. Souza, R. Ribeiro, A. Feitosa, V. Silva, D. Ribeiro, R. Covello de Freitas, M. Lima, N. Soares, R. Valença, and R. Ogava, *Image Reconstruction of Electrical Impedance Tomography Using Fish School Search and Differential Evolution*, 02 2018.

[24] A. Feitosa, R. Ribeiro, V. Barbosa, R. Souza, and W. Dos Santos, "Reconstruction of electrical impedance tomography images using particle swarm optimization, genetic algorithms and non-blind search," 08 2014.

[25] Z. Wei and X. Chen, "Induced-current learning method for nonlinear reconstructions in electrical impedance tomography," *IEEE Transactions on Medical Imaging*, pp. 1–1, 2019.

[27] Z. Wei, D. Liu, and X. Chen, "Dominant-current deep learning scheme for electrical impedance tomography," *IEEE Transactions on Biomedical Engineering*, vol. 66, no. 9, pp. 2546–2555, 2019.

[28] S. Liu, J. Jia, Y. D. Zhang, and Y. Yang, "Image reconstruction in electrical impedance tomography based on structure-aware sparse bayesian learning," *IEEE Transactions on Medical Imaging*, vol. 37, no. 9, pp. 2090–2102, 2018.

[29] Ying Li, Liyun Rao, Renjie He, Guizhi Xu, Qing Wu, Weili Yan, Guoya Dong, and Qingxin Yang, "A novel combination method of electrical impedance tomography inverse problem for brain imaging," *IEEE Transactions on Magnetics*, vol. 41, no. 5, pp. 1848–1851, May 2005.

[30] M. Zhou, "Electrical impedance tomography based on genetic algorithm," *arXiv.org*, 2019. [Online]. Available: http://search.proquest.com/docview/2167517849/

[31] D. W. Marquardt, "An algorithm for least-squares estimation of nonlinear parameters," *Journal of the Society for Industrial Applied Mathematics*, vol. 11, no. 2, pp. 431–441, 1963.

[32] Q. Fan, X. Yan, and Y. Zhang, "Auto-selection mechanism of differential evolution algorithm variants and its application," *European Journal of Operational Research*, vol. 270, no. 2, pp. 636 – 653, 2018.

[33] C. Lin, A. Qing, and Q. Feng, "A comparative study of crossover in differential evolution," *Journal of Heuristics*, vol. 17, no. 6, pp. 675–703, 2011.